High-field magnetization scaling relations for pure and Ni-substituted single-crystal $YBa_2Cu_3O_7$

K. A. Delin* and T. P. Orlando
Department of Electrical Engineering and Computer Science, Massachusetts Institute of Technology, Cambridge, Massachusetts 02139

E. J. McNiff, Jr. and S. Foner
Francis Bitter National Magnet Laboratory, Cambridge, Massachusetts 02139

R. B. van Dover, L. F. Schneemeyer, and J. V. Waszczak
AT&T Bell Laboratories, Murray Hill, New Jersey 07974

(Received 11 March 1992)

Several scaling relations are inferred from magnetization data taken in fields up to 20 T on single crystal $YBa_2Cu_{3-x}Ni_xO_7$ where $0 \leq x \leq 0.03$. A Bean-like critical state exists in the samples at high fields ($\lesssim 20$ T) and low temperatures (4.2 K) regardless of x. Strong systematics are also displayed in the temperature dependent data: it is found that beyond an applied field breakpoint, which itself scales with temperature as $(1-T/T_c)^{3/2}$, all the scaled hysteresis loops decrease in a universal manner. This universal behavior of the normalized magnetization is well described as a hyperbolic function of the normalized applied field. A quantitative study of the dependence of the measured magnetization as a function of the *sweep rate* of the applied field is also presented. The measured magnetization is found to depend logarithmically on the sweep rate. The simplest diffusion models are inadequate to explain the data.

I. INTRODUCTION

Historically, magnetization measurements have played an important role in determining superconducting properties of new materials especially by providing an alternative method to transport measurements for determining critical current densities. Unfortunately, most of the magnetic studies performed on the high-temperature superconductors have been made over a limited applied field range (typically $\lesssim 5$ T). This paper presents a systematic study of the hysteresis loops of high-quality, single-crystal $YBa_2Cu_3O_7$, in both its pure and Ni-substituted forms, made over a wide temperature ($1.4\ \text{K} \lesssim T \lesssim T_c$) and field ($\mu_0 H \lesssim 20$ T) range.

The organization of the paper is as follows. A description of the materials and experiments is given in Sec. II. Section III focuses on low-temperature hysteresis loops made on many different samples with various nickel-substitution levels. It is found that the low-temperature hysteresis loops scale in a Bean-like manner and that this scaling indicates the data of different pure and Ni-substituted single-crystal samples can be compared directly. The temperature dependence of the hysteresis loops is examined in Sec. IV and a universal scaling is found between the normalized magnetization and the normalized applied field. Measurements also reveal that the magnetization is sensitive to the *sweep rate* of the applied field in a systematic, quantifiable manner. This new result, and the related idea of dynamic magnetization, is presented in Sec. V. Finally, the theoretical implications of the data and the scaling rules developed are considered in Sec. VI.

II. MATERIALS AND EXPERIMENTAL PROCEDURE

The data presented here were taken on single-crystal $YBa_2Cu_{3-x}Ni_xO_7$ where x varied from 0.0 (a pure sample) to 0.03. The samples were produced at AT&T Bell Laboratories and were grown from a partially melted CuO-BaO-Y_2O_3 mixture[1] with the addition of small amounts of NiO. The crystals were then annealed 30–90 days in O_2 in order to attain a homogeneous oxygen content. The best experimental evidence[2] indicates that, for low substitutional concentrations in polycrystalline material, the nickel will go nearly uniformly onto both the Cu(1) (chain) and the Cu(2) (plane) sites. Materials analysis, such as electron microprobe, revealed a macroscopically uniform nickel content throughout each of our samples. Thus far it has not been possible to make single crystals with nickel substitution $x > 0.03$ due to the solubility limit of Ni in the material.

The single crystals used in this study were approximately 1 $\text{mm}^2 \times 0.04$ mm with the $\hat{c}$ axis perpendicular to the square face of the sample. Furthermore, the crystals contained the usual twinned boundaries in the $\hat{a}$-$\hat{b}$ plane. In zero field, T_c ranged from 88 to 76 K for $x = 0.0$ and 0.03, respectively. All zero-field resistive transitions were sharp with the 10–90% transition widths less than 1 K suggesting high-quality material.[3,4] The transport properties of these materials, measured in a magnetic field, were discussed previously.[3,4]

The magnetization measurements discussed here are made using a vibrating sample magnetometer (VSM) in dc magnetic fields up to 20 T in water-cooled Bitter magnets at the Francis Bitter National Magnet Laboratory

facility. The system used allows one to measure total moments as small as 5×10^{-7} A-m^2 (5×10^{-4} emu) in fields to 30 T. The flat, platelike single-crystal samples are mounted on the end of the VSM driving rod and thus are oriented with the applied field parallel to the $\hat{c}$ axis. Bulk properties are relatively insensitive to alignment problems because of the weak angular dependence in this orientation.[4] For some of the measurements, the test sample is immersed in liquid helium. By pumping on the helium bath, the temperature could be lowered to approximately 1.4 K. Elevated temperatures are reached by using a variable temperature dewar. In our arrangement, a small, steady stream of helium gas is heated by a set of heating coils which surround both the sample and the detection coils. The heated gas flows over the sample maintaining its temperature. The current in the heater coils is set using a carbon-glass thermometer and stabilized in the field using a capacitance thermometer. Temperatures in this system are stable to within 0.1 K during the measurement of a single hysteresis loop.

The data are obtained by cycling the Bitter magnet from 0 to 20 T, thus generating a hysteresis loop. The sample is centered between the detection coils by maximizing the detected signal in a small applied field before an actual hysteresis loop is generated. As a result, there is always some trapped flux pinned within the superconducting sample before actual data are taken. The magnetization effects of the trapped flux, however, are destroyed by the time the applied field is at 2 or 3 T (or even lower for elevated temperatures) and thus do not influence the high-field data. Typically, the ramp rate used is 66.7 mT/s (4 T/min); unless otherwise specified this rate may be assumed.

The VSM is calibrated against the saturation moment of a known nickel standard at 4.2 K. The sample mass (typically between 100 and 1000 μg) and density (assumed to be approximately 6.4 g/cm^3 regardless of Ni-substitution level) are used to convert the measured sample moment to a magnetization per unit volume.

III. LOW-TEMPERATURE BEAN-LIKE SCALING

Before discussing the data, the differences between the local electromagnetic (microscopic), average electromagnetic (mesoscopic), and thermodynamic (macroscopic) fields must be distinguished.[5] The thermodynamic field $\mathcal{H}$ is defined as the average of the microscopic field $\mathbf{H}$ over the entire body. In this paper, the thermodynamic fields will be independent of space within the body in question. When looking at the general behavior of fields inside a type-II superconductor without focusing on the granularity associated with fluxoid quantization, the mesoscopic field is the relevant quantity. This field $\tilde{\mathbf{H}}$ is the average of the microscopic field $\mathbf{H}$ over distances large compared to the penetration depth (the electromagnetic size of the fluxoid) but small compared to the macroscopic scale, and thus can vary within the superconducting material. Similar quantities can be defined for the current density $\mathbf{J}$, flux density $\mathbf{B}$, and magnetization $\mathbf{M}$. It should be noted that the measured magnetization $\mathcal{M}$ is the *bulk* magnetization and should not be confused with the local magnetization inside the sample.

Traditionally, critical current densities have been extracted from hysteresis loops using two models. The first was developed by Bean[6,7] and is characterized by a hysteresis loop whose width does not vary with applied field once the penetration field H^* is reached. In general, the critical current density J_c is related to the hysteresis loop by

$$J_c=\beta\frac{\Delta\mathcal{M}}{l}\ , \tag{1}$$

where $\Delta\mathcal{M}$ is the (field-independent) width of the hysteresis loop. The factor l represents a geometrical scaling associated with the sample size; in other words, it is the characteristic dimension for the sample. Often l is associated with a specific sample dimension, such as the thickness of a slab or radius of a cylinder, but it can also represent the geometric mean of several dimensions as well. The factor β represents the scaling associated with sample topology. For example, a cylindrical plate has a different β than a long cylinder although l is given by the radius in both cases. If the critical current density is field dependent, it is common to use a second model developed by Kim, Hempstead, and Strnad (KHS).[8,9] Here the mesoscopic critical current density is given by

$$\tilde{J}_c(r)=\frac{\alpha}{|\tilde{B}(r)|+B_0}\ , \tag{2}$$

where $\tilde{B}$ is the mesoscopic flux density in the material. The parameters α and B_0 are found by fitting this expression to the hysteresis loop. Typically, the field dependence of the KHS model is considered in regimes where the applied field is much larger than B_0 so that $\tilde{J}_c\propto 1/|\tilde{B}|$.

The data obtained from measurements on both pure and Ni-substituted $YBa_2Cu_3O_7$ single crystals at 4.2 K appear to be Bean-like (see, for example, Fig. 1). For applied fields greater than a few tesla, the hysteresis loop displays only a weak-field dependence. Indeed, it is not possible to get a satisfactory fit to this data using the KHS model. We consequently assume that the Bean model is valid for higher magnetic fields (J_c is indepen-

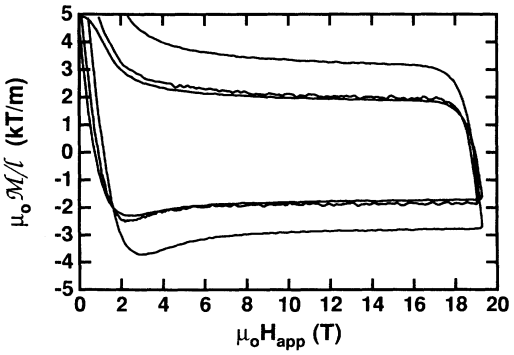

FIG. 1. Scaled magnetization loops at 4.2 K for three $YBa_2Cu_3O_7$ single-crystal samples. These samples are all from batch 2515.

dent of field) and treat the deviant low-field peaks as anomalies.

Equation (1) describes the hysteresis loops under the Bean model. This suggests a simple procedure for scaling the experimental data since all the samples are topologically equivalent (thin plates) and hence have the same β. If the hysteresis loops are scaled by the effective size of the sample l all the magnetization loops should be identical in width for samples of identical stoichiometry.

This quantity l is related to *all* of the various dimensions of the sample. Although some of our samples were square or rectangular plates, most were trapezoidal in shape or more complicated. We thus estimate l by approximating a trapezoidal shape as a rectangle of somewhat reduced dimensions and defining l as the geometric mean of the two resulting sides. Although critical current densities, as deduced from hysteresis loops of superconducting samples of various geometries, have been calculated from the early 1960s (see, for example, Ref. 10), such analytical expressions are not practical here.

The effects of the $YBa_2Cu_3O_7$ anisotropy in the $\hat{a}$-$\hat{b}$ plane also should be included in the Bean model.[11] There are two reasons why we neglect these effects here. First, the $\hat{a}$-$\hat{b}$ anisotropy is small so we approximate the orthorhombic structure with a tetragonal one. Second, because the $\hat{a}$ and $\hat{b}$ axes are rotated as a twin boundary is crossed, any measured bulk property is necessarily an average of both these directions.

Figure 1 compares the scaled hysteresis loops taken at 4.2 K for three undoped samples from the same batch. The values of l for these three samples are 1500, 1180, and 900 μm. (This range of l is typical for our samples.) The data scale well despite the different sample shapes; without this scaling the loop widths vary by a factor of 5.

Similar results are obtained for the $YBa_2Cu_{3-x}Ni_xO_7$ data. For example, the scaled hysteresis loops for four $x=0.01$ samples, all from the same batch, are similar indicating that the scaling procedure is appropriate. These results are also applicable to samples of the same stoichiometry but from different batches. Figure 2 shows that the scaled hysteresis loops are insensitive to the Ni-substitution level as well. Since all the samples have the same topology (same value of β), this implies that Ni substitution has *little or no effect* on the critical current density as deduced from $\mathcal{M}$ at low temperatures. This result is quite surprising since the single crystals had critical temperatures that decreased with increasing amounts of nickel.[3]

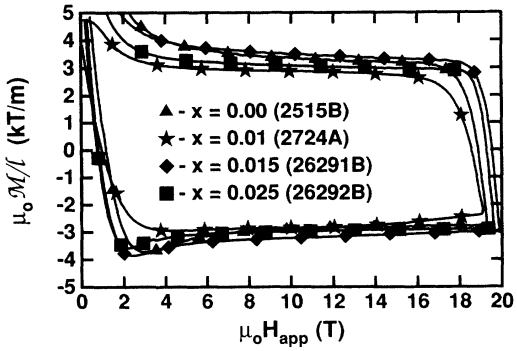

FIG. 2. Scaled magnetization loops at 4.2 K for $YBa_2Cu_{3-x}Ni_xO_7$ single crystals.

Under the Bean model, there is another, self-consistent way to determine the critical current density from the hysteresis loops. This method involves the shielding field H_s which is a measure of how much field is required to fully reverse the critical current density from J_c to $-J_c$ everywhere in the sample. As derived in the Appendix, for a cylindrical plate geometry (radius a, thickness w),

$$J_c(H_s)=\frac{H_s}{w\ln(4a/w)} . \tag{3}$$

Because Eq. (3) depends only weakly on the sample size a, it is essentially an independent way of deducing J_c from the same hysteresis loop that is used to determine J_c from $\Delta\mathcal{M}$.

To compare the two methods, we first examine J_c as predicted by the width of the hysteresis loop, denoted $J_c(\Delta\mathcal{M})$. For a circular cylinder of diameter l, the Bean model gives

$$J_c(\Delta\mathcal{M})=3\frac{\Delta\mathcal{M}}{l} \tag{4}$$

in SI units, when the applied field is oriented along the cylinder's axis.[7] There are two reasons why this topology is a good estimate here. First, we have chosen to treat the dimensions of the sample only in an average sense, so it is self-consistent to smooth out the corners of the actual angled samples. Second, it has earlier been shown that approximating our flat platelike samples by a long cylinder gives valid results.[11]

The calculated values of J_c are given in Table I. $J_c(\Delta\mathcal{M})$ is determined in each case at 4.2 K and approximately 17 T. Since the widths of the hysteresis loops are essentially independent of field, these critical current density values are valid over a wide field range. As shown in the table, $J_c(\Delta\mathcal{M})$ is not sensitive to Ni substitution; its value is approximately 1×10^6 A/cm^2, typical of that obtained by others (Refs. 11–14 and references therein). It

TABLE I. Comparison between the critical current densities for $YBa_2Cu_{3-x}Ni_xO_7$ single crystals as estimated from magnetization and shielding field data. The values given are for applied flux densities (parallel to the $\hat{c}$ axis) of approximately 17 T and at a temperature of 4.2 K.

Sample	x	$J_c(\Delta\mathcal{M})$ (A/cm^2)	$J_c(H_s)$ (A/cm^2)
2515*A*	0.0	0.87×10^6	1.11×10^6
2515*B*	0.0	1.44×10^6	1.51×10^6
2515*C*	0.0	0.93×10^6	1.02×10^6
2724*A*	0.01	1.32×10^6	2.20×10^6
2724*B*	0.01	1.02×10^6	1.40×10^6
2724*C*	0.01	0.87×10^6	1.62×10^6
8541*A*	0.01	1.61×10^6	1.01×10^6
26291*A*	0.015	1.68×10^6	0.88×10^6
26291*B*	0.015	1.50×10^6	1.22×10^6
26292*A*	0.025	1.44×10^6	0.88×10^6
26292*B*	0.025	1.38×10^6	0.91×10^6

should be emphasized, however, that the measurements presented here are over an applied field range that is much greater than those of most other experiments.

The values of $J_c(H_s)$ are also presented in Table I. We again find that the high-field, low-temperature critical current density is approximately 1×10^6 A/cm^2 regardless of the amount of nickel present. Here each sample is approximated as a circular plate with a diameter $2a=l$ and a measured thickness of about 40 μm.

$J_c(\Delta\mathcal{M})$ and $J_c(H_s)$ for each sample generally differ by less than 60%. Because the Bean model of the critical state is applicable at high fields and low temperatures, the depinning force J_cB is linearly dependent upon the applied field. Thus in the low-temperature regime, collective effects among vortices are important. We also expect from the Bean model that the flux profile inside the material is linear. This is consistent with the flux profile observed in powdered samples of $DyBa_2Cu_3O_7$.[15]

IV. TEMPERATURE DEPENDENCE OF HYSTERESIS

Consider the set of hysteresis loops shown in Fig. 3 taken on a $YBa_2Cu_3O_7$ single crystal at various temperatures. The inner loops, taken at temperatures closer to T_c, are similar to those found by others.[16,17] The teardrop shape of these loops is unusual.

We find that the key feature for scaling the curves is the breakpoint as illustrated in Fig. 3. Both the applied field H_b and the magnetization $\mathcal{M}_b$ defining the breakpoint will be important. Notice that here it is only possible to find a breakpoint for the six highest temperature loops. Both H_b and $\mathcal{M}_b$ display a power-law dependence on $(1-t)$ where t is the reduced temperature $t\equiv T/T_c$. This dependence is illustrated in Fig. 4. Although the points do not span several decades, a power-law fit was superior to either linear or exponential fits; the specific fits are given in Table II.

The functional forms are then used to normalize the

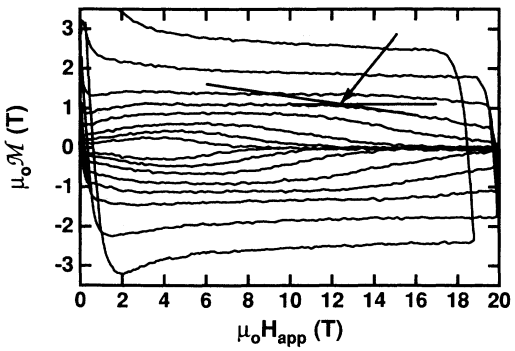

FIG. 3. Hysteresis loops of a $YBa_2Cu_3O_7$ single crystal (sample 2515*B*) taken at different temperatures. The widest loop is measured at a temperature of 12.8 K with progressively smaller loops measured at temperatures of 22.7, 33.2, 40.0, 45.7, 53.5, 59.6, and 65.3 K, respectively. A breakpoint $(H_b,\mathcal{M}_b)|_{40\text{ K}}$ is indicated by the arrow. The straight lines show how the breakpoint is estimated.

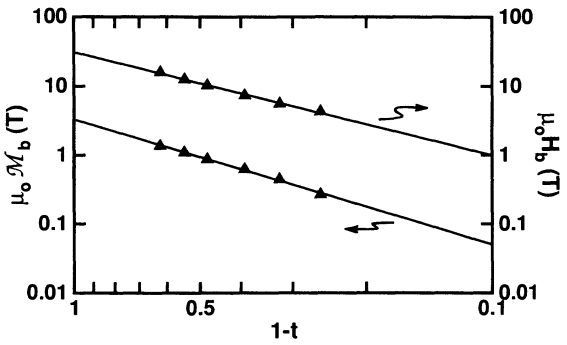

FIG. 4. The dependence of $\mathcal{M}_b$ and H_b on reduced temperature $t\equiv T/T_c$ for the $YBa_2Cu_3O_7$ sample 2515*B*. The fitting parameters are given in Table II.

experimental data so that the normalized magnetization

$$m\equiv\frac{\mu_0\mathcal{M}}{\mu_0\mathcal{M}_b} \tag{5}$$

can be plotted as a function of the normalized applied field

$$h_a\equiv\frac{\mu_0H_{\text{app}}}{\mu_0H_b} \tag{6}$$

for each temperature. The result is shown in Fig. 5: all the loops either scale or continue to extrapolate to the *same* universal curve. Moreover, the two loops which had no discernible breakpoint still fit in the scaled pattern (they are the loops where the applied field never reaches the breakpoint field). For $h_a\lesssim0.7$, the loops do not scale in an overlapping fashion but instead are nested with the highest-temperature loops on the inside.

An analytic expression has been found that quantitatively describes the universal portion of the curves. For $h_a>1$ and $m>0$ the data form a hyperbola with asymptotes of slopes -1 and 0 that intersect at (2,0) (assume mirror image symmetry for $m<0$). This hyperbola is described by the function

$$m=-\frac{h_a-h_0}{2}+\left[\left[\frac{h_a-h_0}{2}\right]^2+\frac{\gamma^2}{2(\sqrt{2}-1)}\right]^{1/2}, \tag{7}$$

where h_0 is the normalized field where the asymptotes intersect (here $h_0=2$) and γ^2 is a fitting parameter determining the eccentricity of the hyperbola. Such an ansatz

TABLE II. Summary of the scaling found for three $YBa_2Cu_{3-x}Ni_xO_7$ single crystals.

Sample	2515*B*	2724*A*	26292*B*
x	0.0	0.01	0.025
T_c (K)	88	82	76
μ_0H_b (T)	$31.2(1-t)^{1.5}$	$9.1(1-t)^{1.5}$	$15.1(1-t)^{1.6}$
$\mu_0\mathcal{M}_b$ (T)	$3.3(1-t)^{1.8}$	$4.5(1-t)^{2.1}$	$2.5(1-t)^{1.6}$
h_0	2	2	2
γ^2	8.9×10^{-3}	1.2×10^{-1}	6.4×10^{-2}

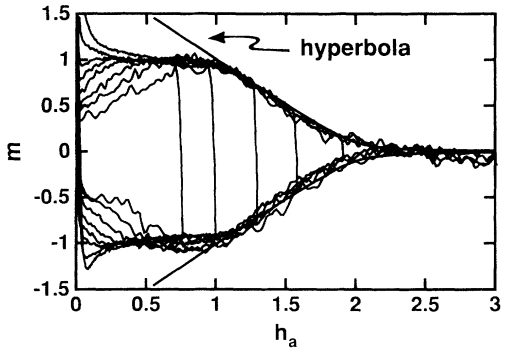

FIG. 5. The same hysteresis loops from Fig. 3 replotted on the normalized axes $h_a \equiv H_{app}/H_b$ and $m \equiv \mathcal{M}/\mathcal{M}_b$. The fitted curve is a hyperbola and accurately describes the decrease in *all* the loops.

produces an excellent fit; the hyperbolas in Fig. 5 have the γ^2 indicated in Table II. This fit implies that in the regime $1.0 < h_a \lesssim 1.8$, m is approximately a linear function of h_a. Under the assumption that a Bean-like model holds in this region, this functional dependence of m means that the critical current density (which is proportional to $2m$) decays linearly with applied field. *This is a completely unexpected result* and, in fact, it contradicts references 18 and 16 where the critical current density (interpreted as the width of the hysteresis loop) is claimed to fall exponentially with field rather than hyperbolically as observed here.

The functional form of Eq. (7) is similar to the magnetization expression obtained from the KHS model. The difference is that the portion of the magnetization loop

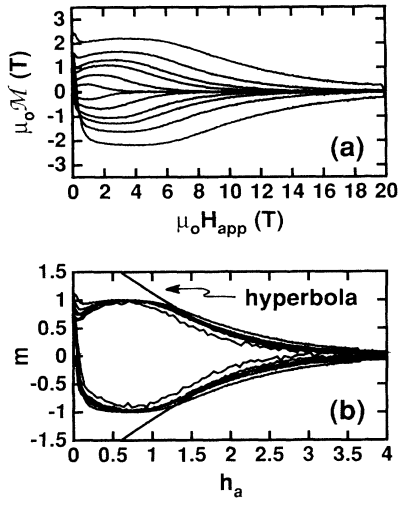

FIG. 6. Hysteresis loops of a $YBa_2Cu_{2.99}Ni_{0.01}O_7$ single crystal (sample 2724*A*). (a) Unscaled data: the widest loop is measured at a temperature of 23.6 K with progressively smaller loops measured at temperatures of 30.5, 35.8, 39.9, 47.8, and 58.1 K, respectively. (b) Scaled data: the fitted curve is a hyperbola and accurately describes the decrease in *all* the loops.

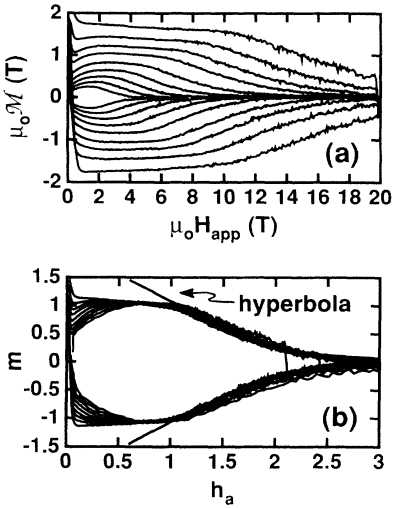

FIG. 7. Hysteresis loops of a $YBa_2Cu_{2.975}Ni_{0.025}O_7$ single crystal (sample 26292*B*). (a) Unscaled data: the widest loop is measured at a temperature of 20.0 K, with progressively smaller loops measured at temperatures of 24.8, 29.2, 33.2, 38.9, 44.0, 48.9, 53.4, and 58.0 K, respectively. (b) Scaled data: the fitted curve is a hyperbola and accurately describes the decrease in *all* the loops.

associated with the second asymptote (the one with finite slope) is never seen in the KHS model, whereas here its presence is clearly discernible (for details see Ref. 19). Whether the similarity in form implies a connection between the KHS model and the data here or is merely coincidence is still not known.

In Sec. III, we saw that the qualitative loop characteristics of samples with different Ni-substitution levels were essentially the same at low temperatures. Here, the higher-temperature scaling and fitting procedure also applies to the Ni-substituted single crystals as can be seen from Figs. 6 and 7. The relevant parameters are given in Table II.

V. SWEEP RATE DEPENDENCE OF HYSTERESIS

It is well established that the phenomenon of flux creep in a constant field for conventional type-II superconductors creates a temporal decay in the bulk magnetization that is proportional to $\ln t$.[20] This decay has been observed in the high-temperature superconductors as well (see, for example, Ref. 21 and references therein). It is not surprising then that early VSM investigations[22,23] demonstrated convincingly that the measured magnetization could be significantly affected ($\sim$20%) by altering the applied field sweep rate. Here, we present a quantitative study of the sweep rate dependence of the hysteresis made on single-crystal samples.

The previously discussed magnetization data were taken at a constant sweep rate of 66.7 mT/s. Figure 8(a) shows the sweep rate dependence of the data. Each notch in the hysteresis loop is obtained by stepping the sweep rate from its nominal value of 66.7 to 33.3 mT/s and then to 16.7, 6.7, and finally 3.3 mT/s after which the

rate is returned to 66.7 mT/s. [An expanded view of a typical notch is shown in Fig. 8(b).] At each step in the sweep rate, the trace responded "instantaneously" (<1 s). In other words, the response was limited by the natural time constants associated with the Bitter magnet system and the recording device. The rate dependence obtained from various notches is shown in Fig. 9. These data are fit by

$$\mathcal{M}=\mathcal{M}_0(H_{\rm app},T)\left[1+C(H_{\rm app},T)\ln\left[\frac{\dot{H}_{\rm app}}{\dot{H}_0}\right]\right], \quad (8)$$

where $\mathcal{M}_0$ is the magnetization associated with the sweep rate $\dot{H}_0$ (here $\dot{H}_0\equiv 66.7$ mT/s). The data taken were insufficient to determine precisely the functional form of $C(H_{\rm app},T)$ although our data show a reasonably linear dependence on applied field (see inset to Fig. 9).

Equation (8) describes unexpected vortex dynamics despite its similarity to the conventional flux creep formation.[20] Specifically, we expect from flux creep that

$$-\frac{1}{\mathcal{M}}\frac{\partial\mathcal{M}}{\partial\ln t}=C' , \quad (9)$$

whereas from Eq. (8) we find

$$\frac{1}{\mathcal{M}}\frac{\partial\mathcal{M}}{\partial\ln\dot{H}_{\rm app}}=C . \quad (10)$$

Equation (10) is not a result of Eq. (9) and this can be demonstrated experimentally as follows. Complete hysteresis loops were taken at the same temperature but with the constant sweep rates 66.7 and 16.7 mT/s. These complete loops match those portions of the notched loop in the regions where the sweep rate was the same even though there was a different time (measured from the start of each set of data) at which the same field magnitude was applied [see Fig. 8(b)].

Further evidence for this novel response comes from examining the shielding field at different sweep rates. Figure 10 shows the response of the shielding field H_s at 4.2 K for two different sweep rates 66.7 and 3.3 mT/s. This data implies that $J_c(H_s)$ is approximately the same value regardless of the sweep rate (note the expanded scale for $\mu_0 H_{\rm app}$), but that $J_c(\Delta\mathcal{M})$ is larger for faster sweep rates. This is consistent with our observation that the rate-dependent vortex dynamics happen on an "in-

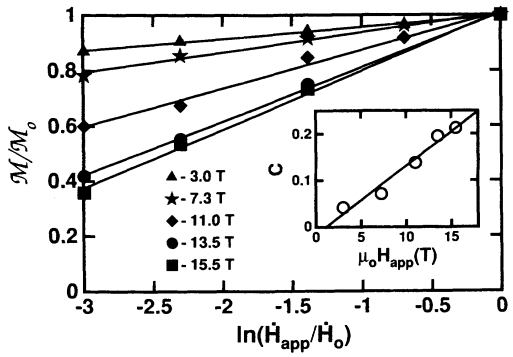

FIG. 9. The scaled magnetization vs the logarithm of the sweep rate. ($\mathcal{M}_0$ is the magnetization at the sweep rate $\dot{H}_0=66.7$ mT/s.) The data is taken on the $YBa_2Cu_{2.975}Ni_{0.025}O_7$ sample 26292*B* at 20 K. Inset: the values of $C=\partial\ln\mathcal{M}/\partial\ln\dot{H}_{\rm app}$ deduced from the data; the dependence with respect to applied field is roughly linear.

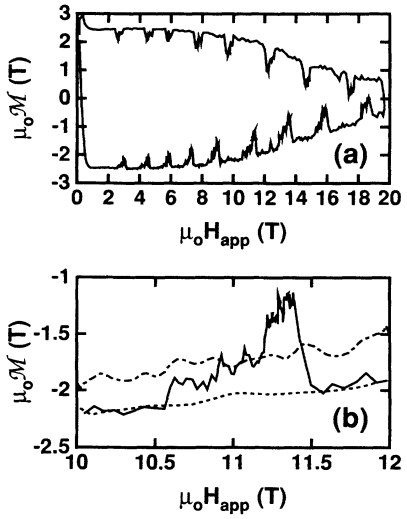

FIG. 8. A typical hysteresis loop showing the dependence of $\mathcal{M}$ on various sweep rates. The data are taken on the $YBa_1Cu_{2.975}Ni_{0.025}O_7$ sample 26292*B* at 20 K. (a) The notched loop. (b) An expanded view of the notch at approximately 11 T. At approximately 10.6 T, the sweep rate is stepped from its nominal value of 66.7 to 33.3 mT/s. The rate is subsequently stepped to 16.7 mT/s at approximately 10.9 T, then to 6.7 mT/s at approximately 11.2 T, to 3.3 mT/s at approximately 11.3 T, and finally returned to 66.7 mT/s at approximately 11.4 T. Each notch in the complete loop is obtained in a similar manner. Smoothed data taken at the constant sweep rates 66.7 (dotted line) and 16.7 mT/s (dash-dotted line) are superimposed.

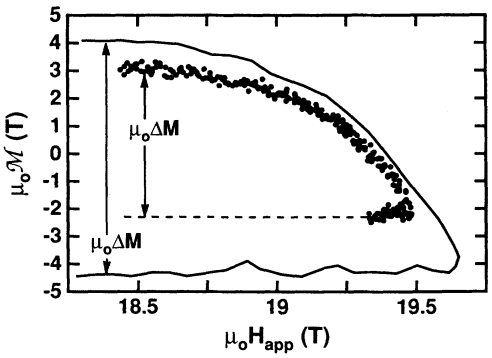

FIG. 10. The expanded portions of two hysteresis loops. These data were taken on the $YBa_2Cu_{2.975}Ni_{0.025}O_7$ sample 26292*B* at a temperature of 4.2 K. The larger loop was taken at a rate of 66.7 mT/s, the smaller loop at a rate of 3.3 mT/s. The vertical arrows indicated the rate-dependent width of the hysteresis loops. In contrast, the shielding field (roughly the horizontal width of the data shown) is nearly independent of sweep rate.

stantaneous" time scale and are different from the flux creep dynamics.

This series of experiments suggests that the magnetization is given by

$$\mathcal{M}=\mathcal{M}_{qe}(H,T)+\mathcal{M}_d(H,\dot{H},T) , \tag{11}$$

where $\mathcal{M}_{qe}$ is the quasiequilibrium magnetization associated with vortex motion similar to conventional flux creep and $\mathcal{M}_d$ is the dynamic magnetization intimately dependent on the sweep rate. This new dynamics should invalidate our previous estimates of the critical current densities made using the width of the hysteresis loop since the dynamic magnetization is not in a critical state, at least within the time scales studied. However, at lower temperatures (4.2 K), $\mathcal{M}_d$ is at most about 20% of the total magnetization $\mathcal{M}$. Consequently, this difference is on the same order as other approximations made and will not significantly affect the previous discussion. Also, it should be pointed out that the quasiequilibrium state *does not* provide the expected Bean-like or KHS-like shape to the hysteresis loop. At whatever sweep rate was used, the hysteresis loop had a teardrop shape for sufficiently high temperatures. This behavior is not expected from any of the classical models.

VI. DISCUSSION

A summary of the experimental results is as follows.

(1) There is no qualitative difference in the magnetization data among the single-crystal samples of $YBa_2Cu_{3-x}Ni_xO_7$ examined here. In addition, there is no systematic quantitative difference as a function of the nickel-substitution level either.

(2) At low temperatures $T \ll T_c$ the measured magnetization can be understood in terms of the Bean model as evidenced by the shape of the hysteresis loops and the self-consistency of $J_c(\Delta\mathcal{M})$ and $J_c(H_s)$.

(3) For $T < T_c$, the magnetization $\mathcal{M}$ is composed of two parts: a quasiequilibrium portion $\mathcal{M}_{qe}$ and a dynamic portion $\mathcal{M}_d$.

(4) In high fields, $\mathcal{M}$ at various temperatures can be scaled accurately with a hyperbolic functional form [see Eq. (7)].

(5) The magnetization increases as the logarithm of the applied field sweep rate [see Eq. (8)].

The rest of this section will examine some possible ways of interpreting these results.

Table II summarizes the temperature dependence of the scaling of the magnetization: all the field breakpoints H_b scale approximately as

$$H_b \propto (1-t)^{3/2} . \tag{12}$$

As discussed in Ref. 24, a characteristic field with this temperature dependence has been associated with an irreversibility line whose existence has been linked to a variety of mechanisms, e.g., the vortex glass, giant flux creep, and vortex lattice melting. Equation (12) always seems to describe a characteristic field in single- and oriented-crystal $YBa_2Cu_3O_7$ regardless of the measurement technique (transport measurements made on these materials showed this dependence as well[3,4]). This dependence also holds for Ni-substituted samples, agreeing with earlier reports.[24] Thus, the breakpoint field H_b may signify a phase boundary in the H-T plane. Indeed, the scaling worked well for applied fields larger than H_b and this is the same regime which displayed the hyperbolic functional form of the magnetization.

As already noted, the quasiequilibrium portion of the magnetization has an unexpected teardrop shape. Interpretation of these magnetization loops of the high-temperature superconductors in terms of a simple diffusion model does not apply to these data as will now be demonstrated.

A model geometry for this analysis is a superconducting slab of thickness $2a$ centered about the y-z plane. The applied field and vortices will all point along the z direction. Because this geometry is one dimensional, we can treat the fields as scalar quantities. We start with the assumption that the observed magnetization is a result of simple diffusion, so the mesoscopic flux density behaves as

$$\frac{\partial}{\partial t}\tilde{B}=D_0\frac{\partial^2}{\partial x^2}\tilde{B} , \tag{13}$$

where D_0 is the diffusion constant, independent of both space and time. If we are referring to classical magnetic diffusion, $D_0=1/(\mu_0\sigma_0)$ where σ_0 is the conductivity of the material. The solution to Eq. (13) is well known (see, for example, Ref. 25). For an infinite slab of thickness $2a$, the response of the slab to an applied ramped field $\dot{H}_{app}$ parallel to its surface is

$$\tilde{B}=\mu_0\dot{H}_{app}\left[t-\sum_{n\ \text{odd}}\frac{4\tau_n}{n\pi}(-1)^{(n-1)/2}\cos\left[\frac{n\pi}{2}\frac{x}{a}\right]\times(1-e^{-(t/\tau_n)})\right] , \tag{14}$$

where the time constant associated with each mode is defined as $\tau_n \equiv 4a^2/D_0n^2\pi^2$. The magnetization in the slab can be expressed as

$$\mu_0\mathcal{M}(t)=\frac{1}{2a}\int_{-a}^{a}\tilde{B}\,dx-\mu_0\dot{H}_{app}t , \tag{15}$$

where the first term on the right-hand side is the thermodynamic flux density $\mathcal{B}$ and the second term is the thermodynamic field $\mathcal{H}$. From Eq. (14), we therefore find

$$\mu_0\mathcal{M}(t)=-\sum_{n\ \text{odd}}2\mu_0\dot{H}_{app}\tau_n\frac{D_0\tau_n}{a^2}(-1)^{(n-1)/2}\times(1-e^{-(t/\tau_n)}) , \tag{16}$$

which is the expected magnetization for an applied ramp if the dominant response is simple diffusion.

The meaning of Eq. (16) can be better appreciated by approximating the expression. The time dependence of the first term (τ_1) is nearly an order of magnitude slower than the next largest term (τ_3) and will thus dominate the time response. We therefore approximate the magnetization by the first term alone,

$$\mu_0 \mathcal{M}(t) \approx -\frac{8}{\pi^2}\mu_0 \dot{H}_{\rm app}\tau_1(1-e^{-(t/\tau_1)}) , \tag{17}$$

and find that the magnetic response to an applied field ramp is diamagnetic reaching its final value in a time of order τ_1. It is significant that for $t \gtrsim \tau_1$, $\mathcal{M}$ is *independent of time* in this model. Equation (17) thus provides a means to estimate τ_1. If $\Delta\mathcal{M}_1$ is the approximate change in magnetization after the system reaches its time-independent final state, then

$$\tau_1 \approx \frac{\pi^2}{8}\frac{\mu_0 \Delta \mathcal{M}_1}{\mu_0 \dot{H}_{\rm app}} . \tag{18}$$

Consequently, we estimate that for the standard sweep rate of 66.7 mT/s, a change in magnetization of 1 T takes about 18.5 s, much longer than actually observed. Moreover, the essential feature of the diffusion response to a ramp, the final time-independent state, is not seen. Recall that at higher fields (where experimentally $\mathcal{M}_{\rm qe} \ll \mathcal{M}_d$), the magnetization decreases hyperbolically. We have therefore shown that the simple diffusion model (D_0 is a constant) is not useful in examining the data.

If a diffusionlike equation provides an adequate phenomenological model, the next step is to make the diffusion coefficient depend, at least implicitly, on space and time (see, for example, Ref. 26 and references therein). The basic premise is to look at the mesoscopic field in terms of the individual fluxoids and then apply standard Boltzmann transport ideas to the particles. In other words, we begin by defining the density of fluxoids as $n = \tilde{B}/\Phi_0$ where Φ_0 is the quantum unit of flux associated with a fluxoid. We write the flux of flux, Γ, as

$$\Gamma = \Phi_0 n \mathbf{v} - \Phi_0 D \nabla n , \tag{19}$$

where the first term represents drift of the fluxoids and the second term represents diffusion. As with classical electron transport, we now describe the drift term as a function of a mobility by examining the force balance on an individual fluxoid. The first assumption is to neglect the fluxoid inertia[27–29] because in all known-type-II superconductors, inertial forces are negligible to damping forces.[30] The resulting force balance yields

$$\tilde{\mathbf{J}} \times \mathbf{\Phi}_0 - \eta \mathbf{v} = 0 , \tag{20}$$

where the first term is the Lorentz-like driving force and the second term is the damping or drag force, quantified by the damping coefficient η. Because the problem is two dimensional, all the flux lines are normal to the plane of motion and so $\mathbf{\Phi}_0 = \Phi_0 \mathbf{i}_z$ where $\mathbf{i}_z$ is normal to the plane. From Ampère's law, the Lorentz-like force term can be rewritten as

$$\tilde{\mathbf{J}} \times \mathbf{\Phi}_0 = -\frac{\Phi_0}{\mu_0}\nabla \tilde{B} \tag{21}$$

since $\tilde{\mathbf{B}}$ only points along $\mathbf{i}_z$. As a result, the velocity can be expressed as

$$\mathbf{v} = -\frac{\Phi_0}{\mu_0 \eta}\nabla \tilde{B} . \tag{22}$$

The proportionality constant between the velocity and the driving term is the mobility μ_m, defined here as

$$\mu_m \equiv \frac{\Phi_0}{\mu_0 \eta} . \tag{23}$$

From Eq. (22), we see that in this model nonlinearities in the flux distribution are unavoidable: both the fluxoid concentration *and* the fluxoid velocity depend on $\tilde{B}$. In fact, conservation of fluxoid particles demands that

$$-\frac{\partial}{\partial t}(\Phi_0 n) = \nabla \cdot \Gamma , \tag{24}$$

which can be written in terms of the mesoscopic field as

$$\frac{\partial}{\partial t}\tilde{B} = \nabla \cdot ([\mu_m \tilde{B} + D]\nabla \tilde{B}) . \tag{25}$$

Writing the Bardeen-Stephen viscosity coefficient in terms of the upper critical field,[5]

$$\eta = \Phi_0 \sigma_0 \mu_0 H_{c2} \tag{26}$$

(where σ_0 is the normal state conductivity), we therefore find

$$\frac{\partial}{\partial t}\tilde{B} = \nabla \cdot \left[\left[\frac{1}{\mu_0 \sigma_0}\frac{\tilde{B}}{\mu_0 H_{c2}} + D \right] \nabla \tilde{B} \right] . \tag{27}$$

This expression is suggestive of the fact that there may be two types of diffusive processes: a "field diffusion," analogous to magnetic diffusion, and a "particle diffusion," analogous to thermal creep of fluxoids as originally suggested by Anderson[31] and augmented by Beasley, Labusch, and Webb[20] and, more recently, by others (see, for example, Ref. 32). Since it is associated with the particle diffusion, we speculate that D is associated with the temporal decay of the quasiequilibrium portion of the magnetization.

We now show that the field diffusion term itself contains enough physics to explain qualitatively the unusual hysteresis data. In this case, we have the nonlinear diffusion equation

$$\frac{\partial}{\partial t}\tilde{B} = \nabla \cdot \left[\left[\frac{1}{\mu_0 \sigma_0}\frac{\tilde{B}}{\mu_0 H_{c2}} \right] \nabla \tilde{B} \right] \tag{28}$$

which must be solved numerically. (The Boltzmann-Matano analytical method[33] uses experimental data to determine a concentration-dependent diffusion coefficient, which here is known to vary linearly.) Moreover, the numerical solution must include the constraint that $|\nabla \tilde{B}| \leq \mu_0 \tilde{J}_c$ if we assume that the material remains superconducting on a mesoscopic scale.

Nevertheless, several important qualitative observations can be made by looking at the linearized form of Eq. (28). Since by definition the spatial average of the mesoscopic field is $\mathcal{B}$, we can write

$$\tilde{B}(x,t) = \mathcal{B}(t) + b'(x,t) , \tag{29}$$

where b' is the mesoscopic perturbation from the average. Using this relation, the nonlinear diffusion equation becomes

$$\frac{\partial}{\partial t}b' = \frac{1}{\mu_0\sigma_0}\frac{\mathcal{B}}{\mu_0 H_{c2}}\nabla^2 b' , \tag{30}$$

where we have assumed that

$$\frac{\partial}{\partial t}\mathcal{B} \ll \frac{\partial}{\partial t}b' . \tag{31}$$

Equation (30) is a simple diffusion expression again, but in terms of the perturbation field. We see that as $\mathcal{B}$ grows monotonically, the diffusion constant grows, and so the time associated with the diffusion decreases. Consequently, we find that the nonlinear diffusion equation qualitatively provides the correct type of behavior; the higher the magnetic field the smaller the magnetization. This expression also qualitatively supports the rate-dependent observations since the slower sweep rates allow the diffusion to catch up to the equilibrium distribution faster. Qualitatively, we see that the flux distribution is "stiffer" at lower applied fields and "softer" at higher ones which allows for the magnetization to grow when ramping down from very high fields. To quantitatively test these ideas requires a full numerical study of Eq. (27).

VII. CONCLUSIONS

Three different scalings of the magnetization data of $YBa_2Cu_{3-x}Ni_xO_7$ single crystals have been developed. The first is a Bean-like scaling that is valid at low temperatures. In this regime, the nickel-substitution levels examined do not change J_c. The second is a temperature-dependent scaling. Beyond a breakpoint field H_b which scales as $(1-T/T_c)^{3/2}$, the magnetization varies hyperbolically with the applied field. The third is a dynamic rate-dependent scaling. Experiments demonstrate that the magnetization is proportional to the logarithm of the applied field sweep rate.

These scaling laws are motivated by two observations. First, the shapes of the hysteresis loops at higher temperatures do not follow the classical shapes as expected from traditional theory. Second, the loops indicate that there is both quasiequilibrium and dynamic fluxoid behavior. Consequently, additional high-field magnetization measurements are warranted. For example, magnetic measurements should be taken on untwinned single crystals to ensure that the dynamic effects are not the result of twin boundaries.

A numerical study should also be made of the nonlinear "field" diffusion relation Eq. (28) that is consistent with the flux limiting condition $|\nabla\tilde{B}| \le \mu_0\tilde{J}_c$. The thermal "particle" diffusion term should be put into the model as well. Indeed, it is tempting to speculate that the "field" and "particle" diffusion map onto the dynamic and quasiequilibrium magnetizations, respectively. Additional work also needs to be done concerning the hyperbolic dependence of the total magnetization on the applied field, Eq. (7). It is not clear whether or not it is coincidence that the classical KHS model also has a magnetization which is hyperbolically dependent on the applied field. It is also possible that the dynamics of the magnetization is best described phenomenologically by a nonlinear viscosity (similar to the stress-strain relationship in a viscoelastic material).

ACKNOWLEDGMENTS

We wish to thank E. H. Frank and S. Kaushik for enjoyable discussions. This work is supported by NSF Grant No. DMR-8802613. The Francis Bitter National Magnet Laboratory is supported by the NSF.

APPENDIX: THE SHIELDING FIELD INTERPRETATION OF J_c

To find the relationship between J_c and the shielding field H_s, consider a thin washerlike disk of superconducting material with outer radius a, inner radius b, and thickness w. (A washerlike geometry is used for convenience only and the limit $b/a \to 0$ will be taken at the end of the calculation.) If we assume that the disk is in a Bean-like critical state, that is, a spatially independent J_c flows everywhere in the sample, then the Biot-Savart law can be used to find the total magnetic field at the center of the coordinate system that is associated with such a current distribution:

$$\tilde{\mathbf{H}}_J(\rho,\phi,z) = \frac{J_c}{4\pi}\int_0^{2\pi} d\phi \int_{-w/2}^{w/2} dz \int_b^a \rho\, d\rho \frac{\mathbf{i}_\phi \times \mathbf{i}_{r'r}}{|r'-r|^2} , \tag{A1}$$

where r is the coordinate of the observer, (0,0,0) here, r' is the coordinate of the source, and $\mathbf{i}_{r'r}$ is the directed vector from r' to r. Since the observer is always at the center of the system,

$$\mathbf{i}_{r'r} = -\frac{\rho}{\sqrt{\rho^2+z^2}}\mathbf{i}_\rho - \frac{z}{\sqrt{\rho^2+z^2}}\mathbf{i}_z \tag{A2}$$

and

$$|r'-r|^2 = \rho^2+z^2 . \tag{A3}$$

Integration therefore yields

$$\tilde{\mathbf{H}}_J(0,0,0) = \frac{J_c w}{2}\ln\left\{\frac{1+[1+(w/2a)^2]^{1/2}}{(b/a)+[(b/a)^2+(w/2a)^2]^{1/2}}\right\}\mathbf{i}_z . \tag{A4}$$

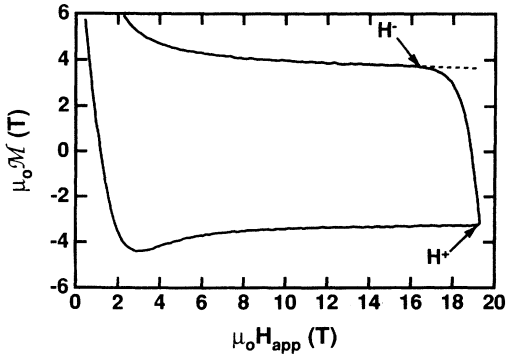

FIG. 11. Details of a hysteresis loop showing how the shielding field H_s is deduced. The shielding field is given by $H_s = H^+ - H^-$.

We wish to examine this expression for thin, solid superconducting disks. Thus we first take the limit $b/a \rightarrow 0$, which can be done exactly, and then linearize the resulting expression consistent with $w \ll a$. Consequently,

$$\tilde{\mathbf{H}}_J(0,0,0)=\frac{J_c w}{2}\ln\left[\frac{4a}{w}\right]\mathbf{i}_z \ . \tag{A5}$$

Suppose the externally applied magnetic field is swept well beyond the penetration field until H^+ is reached as shown in Fig. 11. Because the currents *exclude* the applied field, $\tilde{H}(0,0,0)=H^+-\tilde{H}_J(0,0,0)$ (since all fields are in axially directed, we can suppress the subscript z). Next the applied field is lowered until H^- is reached. This is a special field since it represents the point where all the induced supercurrents *maintain* the field distribution inside the superconductor against the decreasing applied field. In fact, at H^- the field at the center is $\tilde{H}(0,0,0)=H^-+\tilde{H}_J(0,0,0)$. From the critical state model, the local field at the center of the superconductor remains the same during the entire interval $H^- < H_{\rm app} < H^+$ and so equating the two expressions for $\tilde{H}(0,0,0)$, we find $H^+-H^-=2\tilde{H}_J$. Notice that the left-hand side of this expression is our definition of the shielding field H_s. We thus find that for a cylindrical plate geometry

$$J_c=\frac{H_s}{w\ln(4a/w)} \ , \tag{A6}$$

where Eq. (A5) has been used.

*Present address: MIT Lincoln Laboratory, Lexington, MA 02173.

[1]L. F. Schneemeyer, J. V. Waszczak, T. Siegrist, R. B. van Dover, L. W. Rupp, B. Batlogg, R. J. Cava, and D. W. Murphy, Nature **328**, 601 (1987).

[2]F. Bridges, J. B. Boyce, T. Claeson, T. H. Geballe, and J. M. Tarascon, Phys. Rev. B **42**, 2137 (1990).

[3]K. A. Delin, E. J. McNiff, Jr., S. Foner, T. P. Orlando, R. B. van Dover, L. F. Schneemeyer, and J. V. Waszczak, Physica C **162-164**, 719 (1989).

[4]K. A. Delin, T. P. Orlando, E. J. McNiff, Jr., S. Foner, R. B. van Dover, L. F. Schneemeyer, and J. V. Waszczak, IEEE Trans. Magn. **MAG-27**, 1390 (1991).

[5]Terry P. Orlando and Kevin A. Delin, *Foundations of Applied Superconductivity* (Addison-Wesley, Reading, MA, 1991), Secs. 4.5, 6.4 and 7.4.

[6]C. P. Bean, Phys. Rev. Lett. **8**, 250 (1962).

[7]C. P. Bean, Rev. Mod. Phys. **36**, 31 (1964).

[8]Y. B. Kim, C. F. Hempstead, and A. R. Strnad, Phys. Rev. Lett. **9**, 306 (1962).

[9]Y. B. Kim, C. F. Hempstead, and A. R. Strnad, Rev. Mod. Phys. **36**, 43 (1964).

[10]A. M. Campbell and J. E. Evetts, *Critical Currents in Superconductors* (Taylor and Francis, London, 1972), pp. 65–74.

[11]E. M. Gyorgy, R. B. van Dover, K. A. Jackson, L. F. Schneemeyer, and J. V. Waszczak, Appl. Phys. Lett. **55**, 283 (1989).

[12]U. Welp, W. K. Kwok, G. W. Crabtree, K. G. Vandervoort, and J. Z. Liu, Appl. Phys. Lett. **57**, 84 (1990).

[13]P. H. Kes and J. van den Berg, in *Studies of High Temperature Superconductors*, edited by Anant Narlikar (Nova, New York, 1990), Vol. 5, pp. 83–117.

[14]V. M. Pan, in *Studies of High Temperature Superconductors* (Ref. 13), p. 319–359.

[15]M. Daeumling, J. Seuntjens, and D. C. Larbalestier, Appl. Phys. Lett. **52**, 590 (1988).

[16]M. Daeumling, J. M. Seuntjens, and D. C. Larbalestier, Nature **346**, 332 (1990).

[17]J. N. Li, F. R. De Boer, L. W. Roeland, M. J. V. Menken, K. Kadowaki, A. A. Menovsky, and P. H. Kes, Physica C **169**, 81 (1990).

[18]M. M. Fang, V. G. Kogan, D. K. Finnemore, J. R. Clem, L. S. Chumbley, and D. E. Farrell, Phys. Rev. B **37**, 2334 (1988).

[19]K. A. Delin, Ph.D. thesis, Department of Electrical Engineering and Computer Science, Massachusetts Institute of Technology, 1991.

[20]M. R. Beasley, R. Labusch, and W. W. Webb, Phys. Rev. **181**, 682 (1969).

[21]C. W. Hagen and R. Griessen, in *Studies of High Temperature Superconductors* (Ref. 13), Vol. 3, pp. 159–195.

[22]Y. Shapira, C. Y. Huang, E. J. McNiff, Jr., P. N. Peters, B. B. Schwartz, and M. K. Wu, J. Magn. Magn. Mater. **78**, 19 (1989).

[23]L. Půst, M. Jirsa, J. Kadlecová, and S. Durčok, Cryogen. Sept. Suppl. **30**, 886 (1990).

[24]Y. Xu, M. Suenaga, Y. Gao, J. E. Crow, and N. D. Spencer, Phys. Rev. B **42**, 8756 (1990).

[25]Hermann A. Haus and James R. Melcher, *Electromagnetic Fields and Energy* (Prentice-Hall, Englewood Cliffs, NJ, 1989), pp. 434–441.

[26]Ernst Helmut Brandt, Int. J. Mod. Phys. B **5**, 751 (1991).

[27]A. I. Larkin, Y. N. Ovchinnikov, and A. Schmid, Physica B **152**, 266 (1988).

[28]Ulrich Eckern and Albert Schmid, Phys. Rev. B **39**, 6441 (1989).

[29]T. P. Orlando, J. E. Mooij, and H. S. J. van der Zant, Phys. Rev. B **43**, 10218 (1991).

[30]T. P. Orlando and K. A. Delin, Phys. Rev. B **43**, 8717 (1991).

[31]P. W. Anderson, Phys. Rev. Lett. **9**, 309 (1962).

[32]V. M. Vinokur, M. V. Feigel'man, and V. B. Geshkenbein, Phys. Rev. Lett. **67**, 915 (1991).

[33]W. Jost, *Diffusion in Solids, Liquids, Gases* (Academic, New York, 1952), pp. 31–32.